arXiv:1511.00864v1 [cond-mat.mes-hall] 3 Nov 2015

The role of spin-orbit interaction in the ultrafast demagnetization of small iron clusters

Maria Stamenova,[1,*] Jacopo Simoni,[1] and Stefano Sanvito[1]

[1]*School of Physics, AMBER and CRANN Institute, Trinity College, Dublin 2, Ireland*

The ultra-fast demagnetization of small iron clusters initiated by an intense optical excitation is studied with time-dependent spin density functional theory (TDSDFT). In particular we investigate the effect of the spin-orbit interaction on the onset of the demagnetization process. It is found that the initial rate of coherent spin loss is proportional to the square of the atomic spin-orbit coupling constant, λ. A simplified quantum spin model comprising spin-orbit interaction and a local time-dependent magnetic field is found to be the minimal model able to reproduce our *ab initio* results. The model predicts the λ^2 dependence of the onset rate of demagnetization when it is solved either numerically or analytically in the linear response limit. Our findings are supported by additional TDSDFT simulations of clusters made of Co and Ni.

PACS numbers: 75.78.Jp, 75.75.-c, 75.70.Tj, 75.10.Jm

Achieving control over the magnetization dynamics at the femtosecond timescale is a desirable asset for new magnetic data storage technologies. The ultrafast optical demagnetization (UOD) phenomenon, discovered by Beaurepaire *et al*[1], in which an intense femtosecond laser pulse induces an abrupt and dramatic loss of magnetization in a metallic film, initiated what is now the highly active field of femto-magnetism. Typical UOD experiments are based on the pump-probe method, where a femtosecond laser pulse in the optical range (pump) is shed onto the magnetic sample and then a delayed short electromagnetic pulse (probe) is used to detect the magnetic response through possible linear or non-linear magneto-optical effects[2]. By varying the time delay between the pump and the probe the magnetization dynamics can be reconstructed in the time domain over a typical range spanning from a few femtoseconds to a few picoseconds. The rapid demagnetization process that develops over this time can be characterized by two distinct stages: (i) a coherent stage in the first few tens of fs when the light interacts with the electrons and (ii) a relaxation stage when hot electrons and spins interact with each other and with the lattice so to thermalize. Although the role of the particular microscopic spin-flip mechanisms is often unclear and dependent on the details of the magnet investigated, the thermalization process is in general tractable through empirical three-temperature models[1,3], which establish rate equations between the spin, electron and phonon systems. In contrast, theory for the coherent stage is rather unsettled and spans a range of different views (not necessarily mutually exclusive), from relativistic accounts of the direct photon-spin coupling[4] to semi-classical transport models[5].

Experimental works, focussed on the coherent regime, have described a strong dependence of the rate of UOD on the material and, particularly, its spin-orbit coupling (SOC) properties. For instance, it has been reported[6] that materials exhibiting stronger SOC demagnetize significantly faster than lighter ones. The SOC has been identified as a key component enabling UOD also in earlier theoretical works based on model Hamiltonian[7]. Very recently time-dependent spin-density functional theory (TDSDFT) calculations[8] have provided another confirmation of its essential role for the ultrafast laser-induced loss of spin in bulk transition metals. In this letter we seek to gain further understanding of the microscopic mechanisms responsible for the very initiation of the UOD. We employ the only practically-applicable first-principles theoretical framework, the TD(S)DFT[9,10], that allows to simulate the UOD process for real atomic clusters directly in the time domain and for experimentally-relevant times. We demonstrate that the very onset of the demagnetization is triggered by the electronic charge response to the electric field of the pulse. The charge and spin currents generated give rise to a magnetic field which in combination with the SOC facilitates spin flips and global spin decay. We also establish that the initial, coherent demagnetization rate is proportional to the square of the ionic SOC strength for a range of small transition metal clusters.

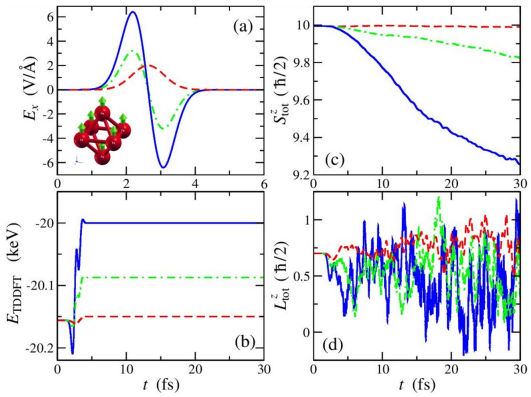

FIG. 1: (Color online) (a) Typical electric field pulses used to excite the Fe_6 cluster (cartooned as inset) and time evolution of the total TDSDFT energy (b), total spin (c) and total KS angular momentum (d) of the cluster when subjected to each of the pulses in panel (a) with corresponding color code on each of the other panels.

In particular, we focus on Fe_6, the geometry and ground state (GS) spin $2S = 20\,\hbar$ of which have been previously predicted by the LSDA[11]. It is well-known that open d-shell systems are problematic to local approximations of the exchange and correlation (XC) functional.

Here, however, our intention is to study the generality of the spin dynamics so that possible quantitative features are not important at this time. We consider the adiabatic temporal extension[12] of the local spin-density approximation (ALSDA), parameterized by Perdew and Wang[13] and implemented in the Octopus code[14].

In all our calculations spin dynamics is initiated by a single intense electric field pulse (we neglect the magnetic field component). We solve the time-dependent Kohn-Sham (KS) equations

$$i\hbar\frac{\partial}{\partial t}\psi_j(\vec{r},t) = H_{\rm KS}(\vec{r},t)\psi_j(\vec{r},t)\,, \tag{1}$$

where $H_{\rm KS}(\vec{r},t)$ is 2×2 matrix in spin space to account for non-collinearity, ψ_j are two-dimensional spinors and we consider the time-dependent KS Hamiltonian with electric field, $\vec{E}(t)$, introduced in the length gauge

$$\begin{aligned} H_{\rm KS}(\vec{r},t) &= -\frac{\hbar^2\nabla^2}{2m} + v_{\rm s}(\vec{r},t) - \frac{2\mu_{\rm B}}{\hbar}\hat{\vec{S}}\cdot\vec{B}_{\rm xc}(\vec{r},t) \quad (2)\\ v_{\rm s}(\vec{r},t) &= \sum_{\vec{R}_I} V_{\rm PP}(|\vec{r}-\vec{R}_I|) + \int d^3r'\frac{n(\vec{r'})}{|\vec{r}-\vec{r'}|} + \\ &\quad v_{\rm xc}(\vec{r},t) + \vec{r}\cdot\vec{E}(t). \quad (3)\end{aligned}$$

We substitute the ionic potentials, centered at each site $\vec{R}_I$, with soft norm-conserving fully relativistic pseudopotentials that reproduce correctly the semi-core and valence wavefunctions beyond a certain core radius[15–17][21]

$$\begin{aligned} V_{\rm PP}(r) &= \sum_l\sum_{m=-l}^{l}\Bigg(\bar{V}_l^{\rm ion}(r) + \frac{1}{4}V_l^{\rm SO}(r) + \\ &\quad V_l^{\rm SO}(r)\hat{\vec{L}}\cdot\hat{\vec{S}}\Bigg)|l,m\rangle\langle l,m|\,. \end{aligned} \tag{4}$$

Here, $\hat{\vec{S}}$ is the spin operator, $\hat{\vec{L}}$ is the angular momentum operator associated to the atomic center, while the scalar part of the pseudopotential $\bar{V}_l^{\rm ion}(r)$ includes the effect of the mass shift and the Darwin term. $V_l^{\rm SO}(r)$ defines the range of the SOC term[22]. Within the adiabatic LSDA, at every time t the XC potentials are calculated through the ground state LSDA exchange-correlation energy functional corresponding to the instantaneous electron charge density $n(\vec{r},t)=\sum_{j\in{\rm occ.}}\psi_j^*(\vec{r},t)\psi_j(\vec{r},t)$ and spin density $\vec{s}(\vec{r},t)=\frac{\hbar}{2}\sum_{j\in{\rm occ.}}\psi_j^*(\vec{r},t)\vec{S}\psi_j(\vec{r},t)$, i.e.

$$v_{\rm xc}(\vec{r},t)=\frac{\delta E_{xc}}{\delta n}\bigg|_{\substack{n(\vec{r},t)\\ \vec{s}(\vec{r},t)}}\,,\quad \vec{B}_{\rm xc}(\vec{r},t)=\frac{\hbar}{2\mu_{\rm B}}\frac{\delta E_{xc}}{\delta\vec{s}}\bigg|_{\substack{n(\vec{r},t)\\ \vec{s}(\vec{r},t)}}\,. \tag{5}$$

For the XC magnetic field the zero-torque theorem holds[18], i.e. $\int d^3r\vec{B}_{\rm xc}(\vec{r})\times\vec{s}(\vec{r})=0$, where the integral is taken over the entire space. In other words, $\vec{B}_{\rm xc}$ cannot produce a global spin torque over the system. The Heisenberg equation of motion for the spin operator leads to a spin continuity equation in the form

$$\frac{d\vec{s}(\vec{r},t)}{dt} = -\nabla\cdot{\rm J}_{\rm KS}(\vec{r},t) + 2\frac{\mu_{\rm B}}{\hbar}\vec{s}(\vec{r},t)\times\vec{B}_{\rm xc}(\vec{r},t) + \vec{\Gamma}(\vec{r},t) \tag{6}$$

where

$$\begin{aligned}\vec{\Gamma}_n(\vec{r},t) &= \sum_{\vec{R}_I}\sum_{\alpha,\beta}\sum_{m,m',l}\epsilon_{njk}V_l^{\rm SO}(|\vec{r}-\vec{R}_I|)\cdot\\ &\quad\cdot\langle\Psi_\alpha^{\rm KS}|l,m',\vec{R}_I\rangle\,\hat{S}^k_{\alpha,\beta}\\ &\quad\langle l,m',\vec{R}_I|\,\hat{L}_I^j\,|l,m,\vec{R}_I\rangle\,\langle l,m,\vec{R}_I|\Psi_\beta^{\rm KS}\rangle\,.\end{aligned} \tag{7}$$

The first term in Eq. (6) can be written as a two components tensor, $\mathrm{J}^{ij}_{\rm KS}(\vec{r},t) = \mathrm{Tr}\left[\hat{S}^i\sum_k(\psi_k^*\partial_j\psi_k - \psi_k\partial_j\psi_k^*)\right]$ is the KS spin-current operator. The second term is the torque exerted locally by $\vec{B}_{\rm xc}(\vec{r},t)$, which vanishes within the adiabatic LSDA ($\vec{B}_{\rm xc}^{ALDA}(\vec{r})\parallel\vec{s}(\vec{r})$). The first term, however, can be rewritten in a form $\frac{2\mu_{\rm B}}{\hbar}\vec{s}\times\vec{B}_{\rm kin}$, where the *kinetic* magnetic field[19] is defined as $\vec{B}_{\rm kin}=\frac{1}{2en}\sum_k\nabla_k(n\nabla_k\vec{s})$. An effective local magnetic field can be defined as $\vec{B}_{\rm eff}(\vec{r},t)=\vec{B}_{\rm kin}(\vec{r},t)+\vec{B}_{\rm xc}(\vec{r},t)$. This field is not necessary locally parallel to $\vec{s}(\vec{r},t)$ and produces a local torque.

The last term in Eq. (6) $\vec{\Gamma}(\vec{r},t)$ is the only source of global spin relaxation in the temporal evolution. Note that in this description the global spin change is only determined by the orbital dependent scattering properties of the non-local component of the atomic pseudopotential as a result of the SOC and it is, therefore, not dependent directly on the Kohn-Sham orbital momentum defined as $\vec{L}_{\rm KS}=\vec{r}\times\vec{J}_{\rm KS}$. Later in this letter we will revisit Eq. (6) and use it as a base for a simplified quantum model for the spin operator.

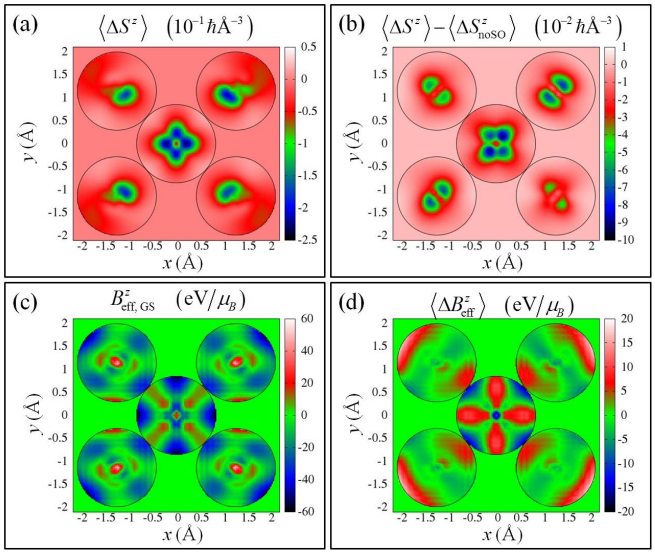

FIG. 2: (Color online) Contour plots of the time-averaged and z-averaged observables evaluated only in spheres of radius 0.85 Å around each atom: (a) the averaged temporal variation of the spin density $S^z(\vec{r})$ with respect to the ground state; (b) difference of the latter and its counterpart in the case of no SOC; (c) the effective magnetic field $B^z_{\rm eff}(\vec{r})$ in the ground state ($t=0$) and (d) the variation of $B^z_{\rm eff}(t)$ with respect to the ground state. See text for details.

Figure 1 shows representative results from the full time-dependent simulations of the dynamics of the Fe_6 cluster. For a range of pulse shapes and amplitudes the

magnetic response is a decay in the global spin expectation value, $S^z(t) = \int d^3r s^z(\vec{r},t)$. The pulse excites the cluster and the rate of the spin decay triggered by the excitation is correlated with the total variation of the TDSDFT energy before and after the pulse (the larger the energy deposited in the cluster, the larger the induced spin-decay rate). Note, that after the pulse the total energy is conserved, Fig. 1(b).

The spatial distribution of the calculated demagnetization is visualized in Fig. 2, where we plot the time and space averaged (along the direction of the symmetry axis of the cluster, z) planar distributions of the temporal variations (with respect to the GS) of the spin-density and the effective magnetic field[23]. It is notable that the negative variation of $s^z(\vec{r})$ is predominantly localized around the atomic centers [panel (a)]. Furthermore, the averaged spin-variation distribution difference between analogous simulations with and without SOC [panel (b)], which approximately represents the global spin loss in the presence of the SOC, is also localized[24]. In particular it is more pronounced along the direction of the bond with the apex atoms, the shortest bond length in the system along the direction of the laser electric field. The effective magnetic field is very inhomogeneous in the GS. Its temporal variation, however, shows a spatial correlation with the variation of the spin density. The regions of decrease of spin density exhibit an increase in $B^z_{\rm eff}(\vec{r})$ (note that in the same regions $B^z_{\rm eff}(\vec{r})$ is mostly negative in the GS). Hence, regions of spin decay are associated with decrease in the absolute value of $B^z_{\rm eff}(\vec{r})$.

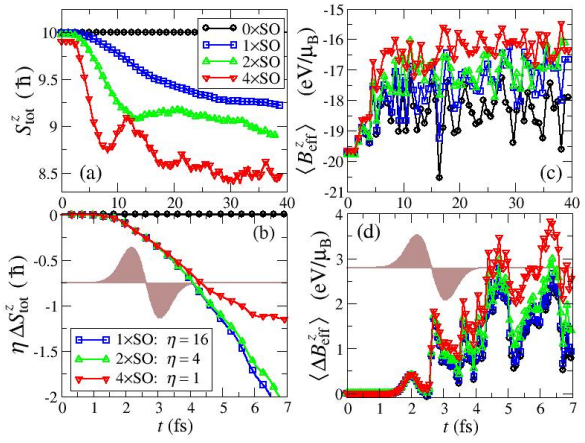

FIG. 3: (Color online) (a) Evolution of global spin expectation value for different factors α in front of the SO term in Eq. (4). (b) Same as in panel (a) but having the GS spin subtracted and $\Delta S^z_{\rm tot}$ values multiplied by $(1/\alpha^2)$. Panels (c) and (d) show the corresponding trajectories of the averaged over the non-overlapping atom-centered spheres $B^z_{\rm eff}(t)$ [see Eq (8)].

As suggested by Eq. (6), the SOC is expected to have a major role in the spin-decay process. In order to extract such effect we have introduced an artificial scaling factor, α, in front of the SOC term of Eq. (4). Depicted in Fig. 3 is the effect on the global spin-variation trajectory of the variation of α from 0 to 4. The rate of spin loss, both pulse-coherent and post-pulse, is strongly affected by the SOC strength with the limit of $\alpha = 0$ (no SOC) resulting in global spin conservation. In panel (b) we have plotted the same spin trajectories after removing their GS offset and scalling them by a factor of $1/\alpha^2$. The overlap of the curves demonstrates that in the initial coherent stage the spin-decay rate scales as the square of the SOC strength.

We now compare the global spin trajectories to those of the $B^z_{\rm eff}$ in the vicinity of the atomic centers. We define a measure of the local variation of the latter as

$$\langle B^z_{\rm eff}(t)\rangle = \sum_i \frac{1}{V_{\Xi_i}} \int_{\Xi_i} B^z_{\rm eff}(\vec{r},t) d^3r \,, \qquad (8)$$

where Ξ_i are non-overlapping atom-centered spheres of radius 0.85 Å for all the quantities plotted in 3(c,d). Although such defined $\langle B^z_{\rm eff}(t)\rangle$ appears noisy due to spatial grid effects, it does show a coherent response to the external field pulse and during this stage it is practically independent of the SOC strength. After the pulse dies out the decrease in the absolute value of $\langle B^z_{\rm eff}(t)\rangle$ correlates to the global spin decay in panel (a), and that is especially notable for higher α. This is related to the fact that practically all the spin loss takes place in the same atomic vicinity regions where $\langle B^z_{\rm eff}(t)\rangle$ is defined.

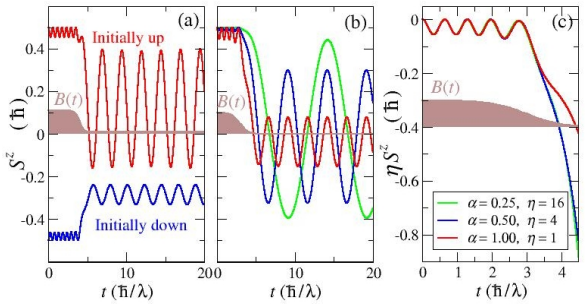

FIG. 4: (Color online) Trajectories for S^z corresponding to the model Hamiltonian of Eq. (9) in the case of (a) having an initial state with spin up or spin down or (b) different values of the SOC (factor α) for an initial spin up. (c) Similarly to Fig. 2(b), the latter trajectories re-scaled by $1/\alpha$. The shaded area is a reference for the temporal profile of $\vec{B} = [0, 0, B(t)]$. The initial orbital momentum state is a linear combination of $l^z = 0, 1, 2$ states.

The insights drawn from Fig. 3 for Fe_6 suggest that the SOC is key in the demagnetization process, which in turn takes place in the vicinity of the atomic sites, i.e. where the SOC is the strongest. Furthermore, we have observed that in the same regions the $B^z_{\rm eff}$ also decays rapidly in time, coherently with the laser field. As a minimal model for understanding the demagnetization process we propose the following spatially homogeneous and time-dependent spin Hamiltonian

$$\hat{H}(t) = \lambda \hat{L}\cdot\hat{S} + \vec{B}(t)\cdot\hat{S} \,, \qquad (9)$$

where λ defines the SOC strength and $\vec{B}(t)$ is a time-dependent magnetic field. This model effectively mimics the local effective spin dynamics at a given point in space arising from the TDSDFT calculation as described by Eq. (6). The basis set used to expand the wavefunction, solution of the corresponding time-dependent

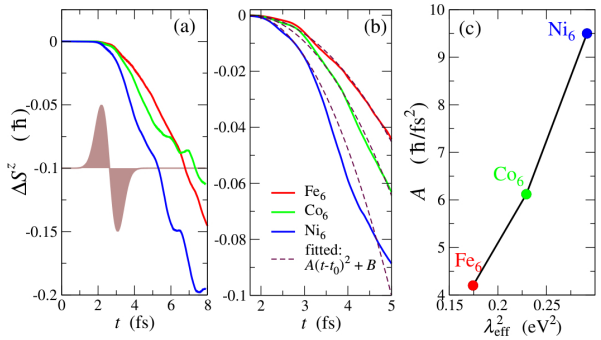

FIG. 5: (Color online) (a) TDSDFT trajectories of S^z_{tot} with respect of the GS for three different clusters: Fe_6, Ni_6 and Co_6, all sharing the same Fe_6 geometry[11]. (b) Closer view into the coherent part of the trajectories where a parabolic decay $[y = A(t-t_0)^2 + B]$ is fitted for each trajectory (dashed curves). (c) The coefficient in the panel (b) fit A versus an effective atomic SOC [Eq. (12)] for each material.

Schrödinger equation, is given by the eigenstates of $\hat{L}^z$ and $\hat{S}^z$, $|l^z, s^z\rangle$. For instance, considering $l = 1$ for the orbital momentum quantum number we can write

$$|\Psi(t)\rangle = \sum_{l^z=-1}^{1} \sum_{s^z=-1/2}^{1/2} c_{l^z,s^z} \, |l^z, s^z\rangle \ , \qquad (10)$$

and solve numerically the 6-dimensional Schrödinger equation to obtain the evolution of the spin observables. The calculated dynamics show that in the absence of SOC there is no spin dynamics regardless of whether or not the initial state is collinear to $\vec{B}(t)$. This is because the spin and orbital angular momenta are decoupled.

In contrast when $\lambda \neq 0$, an initial state with $l^z \neq \pm l$ and a step-like variation of $\vec{B}(t)$ (similarly to $\langle B^z_{\rm eff}(t)\rangle$ in Fig. 3) produce a sharp change in the expectation value of $\hat{S}^z$ (see Fig. 4). In particular, for an initial spin-up state we find a decrease of the S^z expectation value, while an initially down spin-state shows an increase in S^z. In other words, any change of the local magnetic field, combined with the SOC, leads to a decrease in the modulus of the expectation value of the spin of even initially collinear with the field (assumed along the quantization axis) spin-states with $l^z \neq \pm l$ (like the states in the open d-shell of the Fe atoms). In addition, the model reproduces the λ^2 dependence of the coherent demagnetization rate observed in the TDSDFT calculations [Fig. 3(b)]. In Fig. 4(b) and (c) we show that if the SOC strength is rescaled by a factor α the demagnetization curves get steeper by a factor α^2. This property can also be demonstrated analytically by looking at the first order term in the perturbative expansion of the solution $|\Psi(t)\rangle$. For instance, in the case of $|\Psi(0)\rangle = c_1(0)\,|1, -1/2\rangle + c_2(0)\,|0, 1/2\rangle$, the variation of expectation value of $\hat{S}^z$ with respect to the ground state reads

$$\left\langle \hat{S}^z(t) \right\rangle - \left\langle \hat{S}^z \right\rangle_0 = \frac{\lambda^2 t^2}{2} \Big(- \frac{\sqrt{2}}{2} c_1 c_2 - c_1^2 + c_2^2 \Big) \ , \qquad (11)$$

i.e. it scales as λ^2.

As a final proof for the λ^2 dependence of the demagnetization speed, we look at the laser-induced response of clusters analogous to Fe_6 but composed of Co and Ni (we keep the same geometry of Fe_6). We quantify their ionic SOC strength through the following definition

$$\lambda_{\rm eff} = \sum_{l \in {\rm occ.}} \frac{n_l}{n_{\rm tot}} \int V_l^{\rm SO}(\vec{r}) R_l^2(\vec{r}) d^3 r \ , \qquad (12)$$

where n_l are the KS state occupations with l spanning the valence states (in this case $3s, 3p, 3d$ and $4s$), $n_{\rm tot} = \sum_{l \in {\rm occ.}} n_l$, $R_l(\vec{r})$ are the radial pseudo-atomic wavefunctions and $V_l^{\rm SO}(\vec{r}) = \frac{2l}{2l+1} \left[V_{\rm PP}^{l+1/2}(\vec{r}) - V_{\rm PP}^{l-1/2}(\vec{r}) \right]$ is the same object as in Eq. 4 also calculated in the LSDA. By fitting the first few femtoseconds of the demagnetization curve to a quadratic time decay we extract the demagnetization rate of the three different clusters. These show a systematic dependence on $\lambda^2_{\rm eff}$ [see Fig. 5(c)].

In conclusion TD-SDFT calculations obtained with fully relativistic pseudopotentials for transition metal clusters display ultrafast demagnetization with a leading quadratic time dependence and rates ranging between 4 and 10 $\hbar$/fs^2. The phenomenon is then explained in terms of the resulting laser-induced coherent drop of the effective magnetic field. The latter, combined with the SOC which is the strongest in the vicinity of the atomic centers, leads to a local decrease of the expectation value of $\hat{S}^z$. The external electric pulse is therefore only indirectly involved in the demagnetization process, that must be ascribed to the large variations of the effective magnetic field due to excited spin-polarized currents. Furthermore, the onset of the demagnetization shows a clear direct dependence on the ionic SOC properties of the material, scaling quadratically with the SOC strength. Because of the localised nature of this ultrafast demagnetization mechanism, we believe our findings are valid beyond the cluster systems and may provide a formal backing to experimental observations like the comparison of Ni and $CoPt_3$ demagnetization rates in Ref. 6.

This work has been funded by the EU FP7 project CRONOS (grant no. 280879). We gratefully acknowledge the DJEI/DES/SFI/HEA Irish Centre for High-End Computing (ICHEC) for the provision of computational facilities and support and the Trinity Centre for High Performance Computing for technical support.

* Contact email address: stamenom@tcd.ie

[1] E. Beurepaire, J.-C. Merle, A. Daunois, and J.-Y. Bigot, Phys. Rev. Lett. **76**, 4250 (1996).
[2] A.Kirilyuk, A. V. Kimel, and T. Rasing, Rev. Mod. Phys. **82**, 2731 (2010).
[3] B. Koopmans, G. Malinowski, F. D. Longa, D. Steiauf, M. Fhnle, T. Roth, M. Cinchetti, and M. Aeschlimann, Nature Materials **9**, 259 (2010).

[4] Y. Hinschberger and P.-A. Hervieux, Phys. Lett. A **376**, 813 (2012).

[5] . M. Battiato, * K. Carva and P. M. Oppeneer, Phys. Rev. Lett. **105**, 027203 (2010).

[6] J.-Y. Bigot, M. Vomir, and E. Beurepaire, Nat. Phys. **5**, 515 (2009).

[7] G. P. Zhang and W. Hübner, Phys. Rev. Lett. **85**, 3025 (2000).

[8] K. Krieger, J. K. Dewhurst, P. Elliott, S. Sharma, and E. K. U. Gross, J. Chem. Theory Comput. **11**, 4870 (2015).

[9] E. K. U. Gross and W. Kohn, Adv. Quant. Chem. **21**, 255 (1990).

[10] Z. Qian and G. Vignale, Phys. Rev. Lett. **88**, 056404 (2002).

[11] G. L. Gutsev and C. W. Beuschlicher, J. Phys. Chem. **107**, 7013 (2003).

[12] M. A. L. Marques and E. K. U. Gross, *A Primer in Density Functional Theory, Lecture Notes in Physics*, vol. 620 (Springer-Verlag, Berlin, 2003).

[13] J. P. Perdew and Y. Wang, Phys. Rev. B **45**, 13244 (1992).

[14] M. A. L. Marques, A. Castro, G. F. Bertsch, and A. Rubio, Comp. Phys. Comm. **151**, 60 (2003).

[15] C.L.Reis, J.M.Pacheco, and J.L.Martins, Phys. Rev. B **68**, 155111 (2003).

[16] L.Kleinman, Phys. Rev. B **21**, 2630 (1980).

[17] M. J. T. Oliveira and F. Nogueira, Comp. Phys. Comm. **178**, 524 (2008).

[18] K. Capelle, G. Vignale, and B. L. Györffy, Phys. Rev. Lett. **87**, 206403 (2001).

[19] M. I. Katsnelson and V. P. Antropov, Phys. Rev. B **67**, 140406(R) (2003).

[20] J. Zhu, X. W. Wang, and S. G. Louie, Phys. Rev. B **45**, 8887 (1992).

[21] Our fully-relativistic norm-conserving pseudopotentials have been generated with the multi-reference pseudopotential method as implemented in the APE code[17]. This includes, in addition to valence states, also the semi-core ones ($3s$ and $3p$), since semi-core states play an important role in describing the chemical bond and the magnetic properties of transition metal clusters[20].

[22] For values of the radius greater than the range of the SOC component the ionic pseudopotential reduces to a purely local object.

[23] The definitions of the quantities plotted in Fig. 2 are: $\overline{\Delta S^z(x,y)} = \frac{1}{T}\sum_i \int_T dt \int_{z_{i,1}}^{z_{i,2}} dz \left[s^z(x,y,z,t) - s^z(x,y,z,0)\right] / (z_{i,2} - z_{i,1})$ and $\overline{\Delta B^z_{\text{eff}}(x,y)} = \frac{1}{T}\sum_i \int_T dt \int_{z_{i,1}}^{z_{i,2}} dz \left[B^z_{\text{eff}}(x,y,z,t) - B^z_{\text{eff}}(x,y,z,0)\right] / (z_{i,2} - z_{i,1})$, where T is the total simulation time and $z_{i,1}, z_{i,2}$ are functions of (x,y) and belong to one of the non-overlapping atom-centered spheres Ξ_i.

[24] The apparent symmetry breaking is due to the finiteness of the time domain simulation.